A collisional drift wave description of plasma edge turbulence

Masahiro Wakatani
Plasma Physics Laboratory, Kyoto University, Uji 611, Japan

Akira Hasegawa
Bell Laboratories, Murray Hill, New Jersey 07974

(Received 25 August 1983; accepted 5 December 1983)

Model mode-coupling equations for the resistive drift wave instability are numerically solved for realistic parameters found in tokamak edge plasmas. The Bohm diffusion is found to result if the parallel wavenumber is chosen to maximize the growth rate for a given value of the perpendicular wavenumber. The saturated turbulence energy has a broad frequency spectrum with a large fluctuation level proportional to $\bar{\kappa}$ ($=\rho_s/L_n$, the normalized inverse scale length of the density gradient) and a wavenumber spectrum of the two-dimensional Kolmogorov–Kraichnan type, $\sim k^{-3}$.

I. INTRODUCTION

A number of experiments clearly indicates that a tokamak-type plasma with a strong magnetic field exhibits a large level of density fluctuations which increase near the edge.[1,2] The observed frequency spectra are usually broader than the drift-wave frequency, revealing their strongly turbulent nature.[1–4]

Recognizing that the classic weak-turbulence theory fails to explain these results, Fyfe and Montgomery[5] as well as Hasegawa, Kodama, and Maclennan[6] have presented theories of strongly turbulent drift waves based on the model equation derived by Hasegawa and Mima.[7] It was found that the wavenumber spectrum rotates from that peaked in the azimuthal direction to that peaked in the radial direction[6] and that the spectrum obeys the two-dimensional Kolmogorov–Kraichnan law[5,8] ($\sim k^{-3}$).

The importance of mode couplings in such strongly turbulent plasmas are now being recognized by many authors. In particular, Waltz[9] as well as Terry and Horton[10] have made extensive numerical studies of the spectrum evolution based on model mode-coupling equations and have successfully demonstrated that a broad frequency spectrum in fact originates from these models.

To describe the high level of observed turbulence near the plasma edge, Hasegawa and Wakatani have derived model mode-coupling equations based on collisional drift waves and numerically solved them. The wavenumber spectrum of the turbulence is found to exhibit an inverse cascade at large wavenumbers and forms an isotropic, two-dimensional Kolmogorov–Kraichnan spectrum, k^{-3}. The turbulence has a broad frequency spectrum with a large saturation level and produces a Bohm-type particle diffusion.

In this paper, these calculations are extended to include the realistic parameters in the density gradient, viscosity and the ion Landau damping in tokamak edge plasmas. The mode-coupling equations include resistivity which is responsible for the instability and the viscosity which is responsible for the dissipation. The saturation of the instability is found to take place only when both the viscosity *and* the modes with both $k_y > 0$ and $k_y < 0$ are included, where k_y is the wavenumber in the y direction. This means that the saturation can occur by the excitation of waves in the direction of the ion diamagnetic drift.

When the parameter $C_1 \equiv k_z^2 v_{T_e}^2/\nu_e \omega_{ci}$ is chosen such that it maximizes the growth rate of the instability for the particular perpendicular wavenumber of the mode of the perturbation, both the particle flux $\bar{\Gamma}$ and the saturated fluctuation energy $E_{\rm sat}$ (rather than the density fluctuation) are found to be proportional to $\bar{\kappa}$, where $\bar{\kappa}$ is the scale length of the density gradient normalized by ρ_s. From this particle flux, a Bohm-type diffusion coefficient is obtained. The coefficient obtained in the present calculation using parameters close to the real experiment is found to be smaller than the previous model calculation with the fairly large viscosity and $\bar{\kappa}$.[11] For other choices of C_1, e.g., $C_1 = $ const. or $C_1 \propto \bar{\kappa}$, these scalings were not found. The interesting point is that, when C_1 is made large for the long-wavelength region, the density fluctuation excited by the inverse cascade process follows the Boltzmann distribution and the resultant particle flux becomes fairly small.

The particle flux is determined by the phase difference between the density and the potential fluctuations which is proportional to $\bar{\kappa}$. The energy conservation relation for the model equations gives the estimate $\partial E/\partial t \propto \bar{\kappa}\bar{\Gamma} \propto \bar{\kappa}^2$. The saturation time found from the numerical calculations is inversely proportional to $\bar{\kappa}$. This explains our finding, $E_{\rm sat} \propto \bar{\kappa}$.

When electron temperature increases at the edge region, the parameter C_1 becomes large since $C_1 \propto v_{T_e}^2/\nu_e \propto T_e^{5/2}$. In the tokamak discharge with a divertor configuration, the electron temperature near the edge can be made to increase due to the decrease of particle recycling in the scrape-off region. Our numerical result which shows that the particle flux decreases for a larger value of C_1 in the long-wavelength region supports the evidence of better confinement in the H-mode discharges recently found in the ASDEX tokamak.[12]

II. MODEL MODE-COUPLING EQUATIONS

We consider an edge plasma where the temperature is sufficiently low such that the electron mean free path is shorter than qR, where q is the safety factor and R is the major radius. Then the electron Landau damping becomes

 0031-9171/84/030611-08$01.90

less important that the collisional damping, yet we assume that the parallel heat conducivity is sufficiently large that the electrons may be treated as an isothermal fluid along the direction of the magnetic field. These conditions are met if $\omega/\nu_e \ll v_{T_e}^2 k_z^2/\nu_e^2 \lesssim O(1)$, where ω is the typical frequency of the turbulence, ν_{ei} is electron collision frequency, v_{T_e} is the thermal speed, and $k_z \simeq 1/qR$. The resulting mode-coupling equations significantly simplify the earlier attempt for resistive drift wave turbulence.[13] Furthermore, we assume that the electron temperature gradient is much smaller than the density gradient which is supported by the experimental evidence.

We treat ions as a two-dimensional warm fluid with ordering similar to that of the Hasegawa–Mima equations,[7] except for the case where the ion Landau damping is included. The equations for the ion vorticity $\nabla\times\mathbf{v} = (\nabla^2\phi/B_0)\hat{z}$ is then given by

$$\frac{d}{dt}\left(\frac{\nabla^2\phi}{B_0\omega_{ci}}\right) = \frac{1}{en_0}\frac{\partial}{\partial z}J_z + \mu\nabla^2\left(\frac{\nabla^2\phi}{B_0\omega_{ci}}\right), \tag{1}$$

where J_z is the perturbed current density in the $\hat{z}$ direction, ϕ is the electrostatic potential, and μ is the kinematic ion viscosity coefficient ($\mu = 3T_i\nu_{ii}/10m_i\omega_{ci}^2$). The current density J_z consists of the electron J_z^e and ion J_z^i components. We consider that the major contribution of the ion current density is the dissipation of the vorticity through the ion Landau damping which occurs when the drift wave frequency $\omega_*(k_\perp)$ is comparable to $k_z v_{T_i}$, where $k_z \simeq 1/qR$ and v_{T_i} is the ion thermal speed. Then

$$\frac{1}{en_0}\frac{\partial J_z^i}{\partial z} \simeq \omega_*(k_\perp)\frac{T_i}{T_e}\frac{e\phi}{T_e}, \quad \text{if } \omega_*(k_\perp) \simeq \frac{v_{Ti}}{qR},$$
$$= 0, \quad \text{if } \omega_*(k_\perp) > v_{Ti}/qR. \tag{2}$$

The convective derivative is

$$\frac{d}{dt} = \frac{\partial}{\partial t} - \frac{\nabla\phi\times\hat{z}}{B_0}\cdot\nabla, \tag{3}$$

where $\hat{z}$ is the unit vector in the direction of the magnetic field. The continuity equation relates the number density $n(=n_0+n_1)$ to the electron current density

$$\frac{d}{dt}(n_0+n_1) = \frac{1}{e}\frac{\partial}{\partial z}J_z^e, \tag{4}$$

where $n_0(x)$ are the equilibrium density which varies in the x direction. The assumption of the isothermal electron fluid relates J_z^e to n_1 and ϕ through the electron equation of motion in the $\hat{z}$ direction,

$$J_z^e = \frac{T_e}{e\eta}\frac{\partial}{\partial z}\left(\frac{n_1}{n_0} - \frac{e\phi}{T_e}\right). \tag{5}$$

By eliminating J_z^e from Eqs. (4) and (5) we can construct coupled nonlinear equations for ϕ and n_1. If we use the normalization $e\phi/T_e \equiv \phi$, $n_1/n_0 \equiv n$, $\omega_{ci}t = t$ and $x/\rho_s \equiv x$, the coupled equations become

$$\left(\frac{\partial}{\partial t} - \nabla\phi\times\hat{z}\cdot\nabla\right)\nabla^2\phi = \bar{C}_1(\phi - n) + C_2\nabla^4\phi + C_3\phi, \tag{6}$$

and

$$\left(\frac{\partial}{\partial t} - \nabla\phi\times\hat{z}\cdot\nabla\right)(n + \ln n_0) = \bar{C}_1(\phi - n), \tag{7}$$

where

$$\bar{C}_1 = -\frac{T_e}{e^2 n_0\eta\omega_{ci}}\frac{\partial^2}{\partial z^2}, \quad C_2 \equiv \frac{\mu}{\rho_S^2\omega_{ci}},$$
$$C_3 = \frac{\omega_*}{\omega_{ci}}\frac{T_i}{T_e}, \quad \text{if } \omega_* = \frac{v_{Ti}}{qR} \tag{8}$$
$$= 0 \quad \text{otherwise.}$$

The conservation laws for the energy E and the potential enstrophy U can be constructed from Eqs. (6) and (7),

$$\frac{1}{2}\frac{\partial}{\partial t}\int[n^2 + (\nabla\phi)^2]dV$$
$$\equiv \frac{\partial}{\partial t}E(t)$$
$$= -C_1'\int\left(\frac{\partial n}{\partial z} - \frac{\partial\phi}{\partial z}\right)^2 dV - C_2\int(\nabla^2\phi)^2 dV$$
$$- \int n(\hat{z}\times\boldsymbol{\kappa})\cdot\nabla\phi\, dV, \tag{9}$$

and

$$\frac{1}{2}\frac{\partial}{\partial t}\int(\nabla^2\phi - n)^2 dV$$
$$\equiv \frac{\partial}{\partial t}U(t)$$
$$= -C_2\int(n - \nabla^2\phi)\nabla^4\phi\, dV - \int n(\hat{z}\times\boldsymbol{\kappa})\cdot\nabla\phi\, dV. \tag{10}$$

Here $\boldsymbol{\kappa}(= -\rho_s\nabla\ln n_0 > 0)$ shows the normalized density gradient vector, $C_1' = C_1/k_z^2$, and C_3 is neglected for simplicity.

Near the plasma edge, we assume that the density gradient has a constant value which is equivalent to an exponential density profile. Then Eqs. (6) and (7) become uniform in space. These equations show that the nonlinear evolution of the resistive drift wave is completely characterized by only three parameters $\kappa\rho_S$, C_1 and C_2, when the ion Landau damping term C_3 is neglected. Under the same assumption the particle flux in the x direction is given by

$$\bar{\Gamma} = -\left\langle n\frac{\partial\phi}{\partial y}\right\rangle = -\int n(\hat{z}\times\hat{\kappa})\cdot\nabla\phi\, dV, \tag{11}$$

where $\hat{\kappa}$ denotes the unit vector of the density gradient. We note that the unnormalized particle flux is given by $\Gamma = n_0 c_s\bar{\Gamma}$. By use of Eqs. (9) to (11), we can find the relations

$$\frac{\partial}{\partial t}E(t) = -C_1'\int\left(\frac{\partial n}{\partial z} - \frac{\partial\phi}{\partial z}\right)^2 dV$$
$$- C_2\int(\nabla^2\phi)^2\, dV + \bar{\kappa}\bar{\Gamma},$$

and (12)

$$\frac{\partial}{\partial t}U(t) = -C_2\int(n - \nabla^2\phi)\nabla^4\phi\, dV + \bar{\kappa}\bar{\Gamma}.$$

Here $\bar{\kappa}$ is the magnitude of $\boldsymbol{\kappa}$. The relation (12) shows that the enstrophy does not saturate if $C_2 = 0$ and $\bar{\Gamma} \neq 0$ (or $n \neq \phi$). In the numerical calculations, we included viscosity to ensure the saturation. We note that at saturation, the particle flux is

given by

$$\bar{\Gamma} = \frac{C_2}{\bar{\kappa}} \int (n - \nabla^2 \phi) \nabla^4 \phi \, dV$$

$$= \frac{C_1'}{\bar{\kappa}} \int \left(\frac{\partial n}{\partial z} - \frac{\partial \phi}{\partial z} \right)^2 dV + \frac{C_2}{\bar{\kappa}} \int (\nabla^2 \phi)^2 dV. \quad (13)$$

Thus in the presence of C_1 and C_2, a stationary particle flux Γ is produced while both the energy and enstrophy are saturated.

The dispersion relation for the resistive drift wave[14] is obtained from Eqs. (6) and (7)

$$\omega^2 + i\omega(b + k^2 C_2) - ib\omega_* - [k^4/(1 + k^2)] b C_2 = 0,$$

where

$$b = C_1(1 + k^2)/k^2, \quad \omega_* = k_y \bar{\kappa}/(1 + k^2).$$

If C_2 is ignored the solution is

$$\omega = \tfrac{1}{2}[- ib + ib\,(1 - 4i\omega_*/b)^{1/2}]. \quad (14)$$

If $b \gg w^*$ is assumed,

$$\omega \simeq \omega_* + i\omega_*^2/b. \quad (15)$$

The maximum growth rate is found for $b \simeq 4\omega^*$. In terms of C_1, the condition of the maximum growth rate becomes

$$C_1 = 4k^2 k_y \bar{\kappa}/(1 + k^2)^2. \quad (16)$$

For a fixed value of resistivity, C_1 is proportional to k_z^2. Since the plasma can choose any parallel wavenumbers, excitations of waves with k_z which satisfies Eq. (16) for a given value of $k_\perp$ are most likely to occur, provided that the plasma remains collisional for this value of k_z.

III. NUMERICAL CALCULATIONS

By assuming that the density gradient has a constant value (which is equivalent to an exponential density profile), Eqs. (6) and (7) become uniform in space. This means we can solve these equations with a periodic boundary condition. Thus we adopt the Fourier series expansion with the wavenumber vector $\mathbf{k} = (lk_{x0}, mk_{y0})$, where l and m are integers and k_{x0} and k_{y0} are the minimum wavenumbers in the x and the y directions, respectively. The parallel wavenumber is implicitly included in C_1.

Then, the Eqs. (6) and (7) can be written as

$$\frac{\partial n_{\mathbf{k}}^C}{\partial t} = \sum_{\mathbf{k}'+\mathbf{k}''=\mathbf{k}} \frac{1}{2} (\phi_{\mathbf{k}'}^C n_{\mathbf{k}''}^C - \phi_{\mathbf{k}'}^S n_{\mathbf{k}''}^S)(k_x' k_y'' - k_x'' k_y')$$

$$+ k_y \bar{\kappa} \phi_{\mathbf{k}}^S - C_1(n_{\mathbf{k}}^C - \phi_{\mathbf{k}}^C), \quad (17)$$

$$\frac{\partial n_{\mathbf{k}}^S}{\partial t} = \sum_{\mathbf{k}'+\mathbf{k}''=\mathbf{k}} \frac{1}{2} (\phi_{\mathbf{k}'}^S n_{\mathbf{k}''}^C + \phi_{\mathbf{k}'}^C n_{\mathbf{k}''}^S)(k_x' k_y'' - k_x'' k_y')$$

$$- k_y \bar{\kappa} \phi_{\mathbf{k}}^C - C_1(n_{\mathbf{k}}^S - \phi_{\mathbf{k}}^S), \quad (18)$$

$$\frac{\partial \phi_{\mathbf{k}}^C}{\partial t} = \sum_{\mathbf{k}'+\mathbf{k}''=\mathbf{k}} \frac{1}{2} (\phi_{\mathbf{k}'}^C \phi_{\mathbf{k}''}^C - \phi_{\mathbf{k}'}^S \phi_{\mathbf{k}''}^S)(k_x' k_y'' - k_x'' k_y')$$

$$\times \frac{k_x''^2 + k_y''^2}{k_x^2 + k_y^2} + C_1 \frac{n_{\mathbf{k}}^C - \phi_{\mathbf{k}}^C}{k_x^2 + k_y^2} - C_2(k_x^2 + k_y^2)\phi_{\mathbf{k}}^C$$

$$- C_3[1/(k_x^2 + k_y^2)]\phi_{\mathbf{k}}^C, \quad (19)$$

and

$$\frac{\partial \phi_{\mathbf{k}}^S}{\partial t} = \sum_{\mathbf{k}'+\mathbf{k}''=\mathbf{k}} \frac{1}{2} (\phi_{\mathbf{k}'}^S \phi_{\mathbf{k}''}^C + \phi_{\mathbf{k}'}^C \phi_{\mathbf{k}''}^S)(k_x' k_y'' - k_x'' k_y')$$

$$\times \frac{k_x''^2 + k_y''^2}{k_x^2 + k_y^2} + C_1 \frac{n_{\mathbf{k}}^S - \phi_{\mathbf{k}}^S}{k_x^2 + k_y^2}$$

$$- C_2(k_x^2 + k_y^2)\phi_{\mathbf{k}}^S - C_3[1/(k_x^2 + k_y^2)]\phi_{\mathbf{k}}^S, \quad (20)$$

where the superscripts S and C show a sine series and a cosine series, respectively.

We solved Eqs. (17) and (20) numerically to study the nature of the turbulence and the resultant particle diffusion for various values of $\bar{\kappa}$ and C_2. The parameter C_1 is chosen in several ways as will be shown later. The parameter C_3 which characterizes the ion Landau damping is included for one series of the calculations.

The number of modes used in the calculation is typically 24×24 and $k_{x0} = k_{y0} = 2\pi/32$. The integration time step is taken to be $1/1.25 \sim 1/20$ which is chosen according to the linear growth rate (or according to the value of $\bar{\kappa}$). The numerical error is checked with the energy conservation law, Eq. (9) and is kept within 5%.

The first problem is to study the saturation of the linearly unstable drift waves. Here we chose C_1 according to the relation (16). When we start from an initial condition of $n_{\mathbf{k}} = \phi_{\mathbf{k}}$ and $\phi_{\mathbf{k}} = 0.005/(1 + k^2)^{1/2}$ for all perturbations, the saturation in the total energy $E(t)$ is found to appear at $t \simeq 150$ (see Fig. 1). After the saturation, $E(t)$ is found to oscillate around the saturation level. In order to examine a saturation mechanism, we limited the perturbation to $k_y > 0$ throughout a calculation. In this case the total energy did not saturate (see Fig. 2). As the third case, $k_y > 0$ was imposed only to the initial pertubations, but $k_y < 0$ allowed later. In this case the saturation was found to occur as shown in

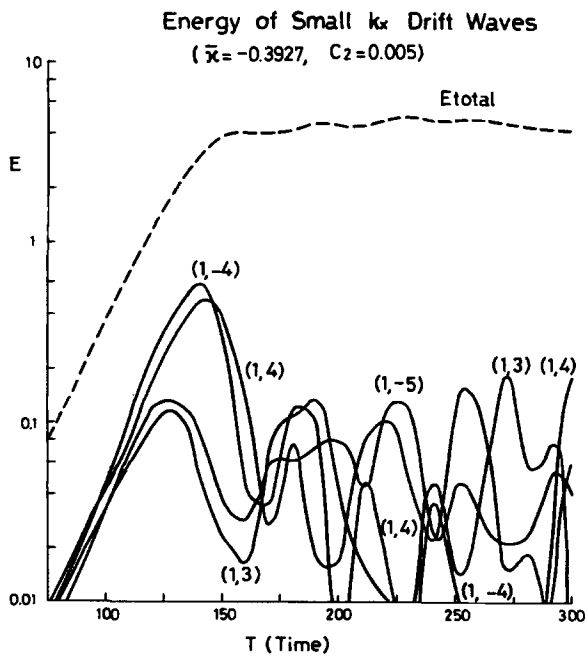

FIG. 1. Temporal behaviors of the total energy, Eq. (9), and the energy of different Fourier modes (k_x, k_y). The saturation is clearly visible.

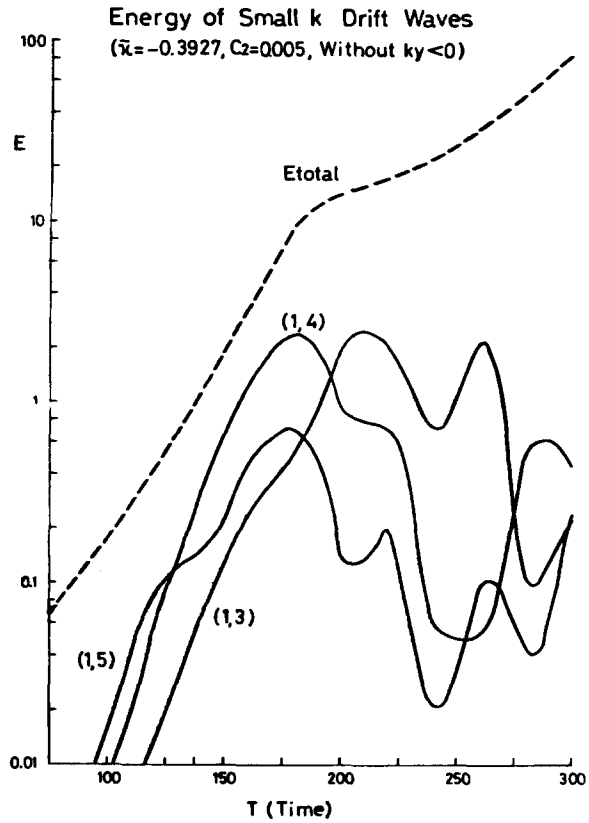

FIG. 2. Temporal behaviors of the total energy and the energy of different Fourier modes in which only modes with $k_y > 0$ are allowed. The saturation is not observed in this case.

Fig. 3. Therefore it is clear that an existence of modes with $k_y < 0$ (the modes which propagate in the direction of the ion diamagnetic drift) is essential for the saturation.

Figure 4 shows the dependence of the saturated energy

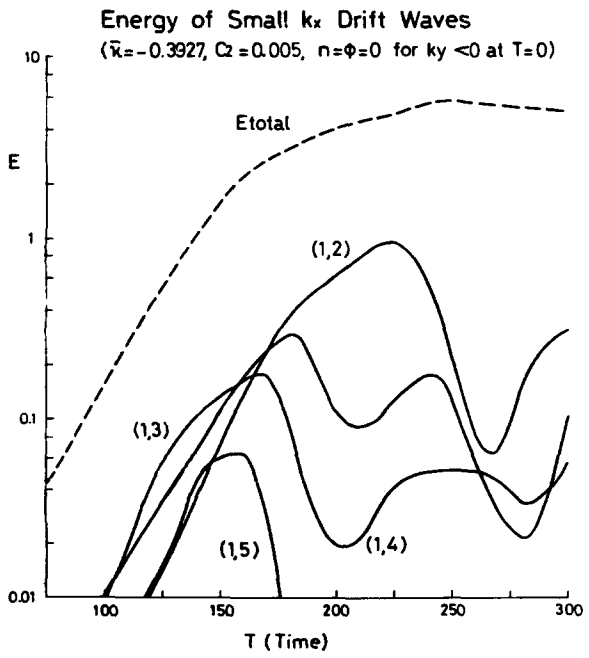

FIG. 3. Temporal behaviors of the total energy and the energy of different Fourier modes in which modes with $k_y < 0$ are absent only at $T = 0$. The saturation is observed in this case.

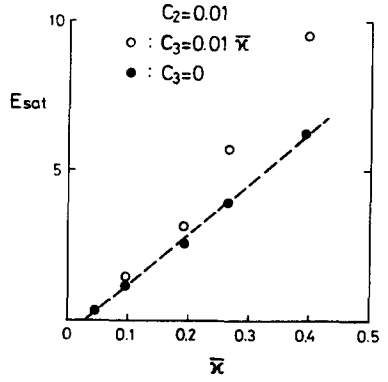

FIG. 4. Dependency of the saturation energy on $\bar{\kappa}$ for a fixed large value of C_2. The circles (dots) are the results with (without) the ion Landau damping.

E_{sat} on $\bar{\kappa}$. E_{sat} is found to increase linearly with $\bar{\kappa}$, but for the small $\bar{\kappa}$ regime the resistive drift wave instability is suppressed by the assumed viscosity as is seen in the linear dispersion relation (13) and E_{sat} goes to zero. Therefore the empirical relation $E_{sat} \simeq 6\bar{\kappa}\,(1 + 140\,C_2)$ and $\bar{\Gamma} \simeq \bar{\kappa}\,(1 + 60 \times C_2)$ presented in our earlier work[11] is found not applicable to the small $\bar{\kappa}$ regime.

Here we used a smaller viscosity parameter C_2 to study the saturation of the unstable resistive drift waves in the small $\bar{\kappa}$ regime. For example, the typical parameter of the Caltech Research Tokamak[1,11] is $\bar{\kappa} \sim 0.02$ and $C_2 \sim (1 \sim 5) \times 10^{-4}$ depending on the ion temperature and the effective charge Z_{eff}. The results for $C_2 = 5 \times 10^{-4}$ are shown in Fig. 5. There exists still a linear relation between E_{sat} and $\bar{\kappa}$. However, the coefficient became smaller. Figure 5 gives $E_{sat} \simeq 1.3\bar{\kappa}$ for this case. Compared to the previous estimation, $E_{sat} \simeq 6\bar{\kappa}$, the saturation level decreases by about factor 5.

It has been shown[11] that the wavenumber spectrum of the energy is seen to form an inverse cascade in the y direction from a peaked spectrum and to cascade to a large wavenumber in the x direction, a tendency qualitatively similar to

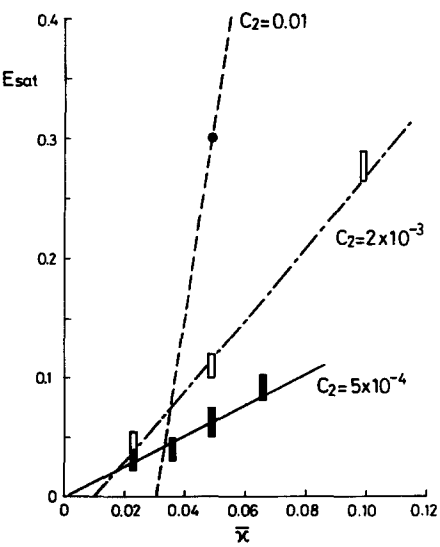

FIG. 5. Dependency of the saturation energy on $\bar{\kappa}$ for a fixed small value of C_2. For a sufficiently small value of C_2, $E_{sat} \propto \bar{\kappa}$ is observed to a small (realistic) value of $\bar{\kappa}$.

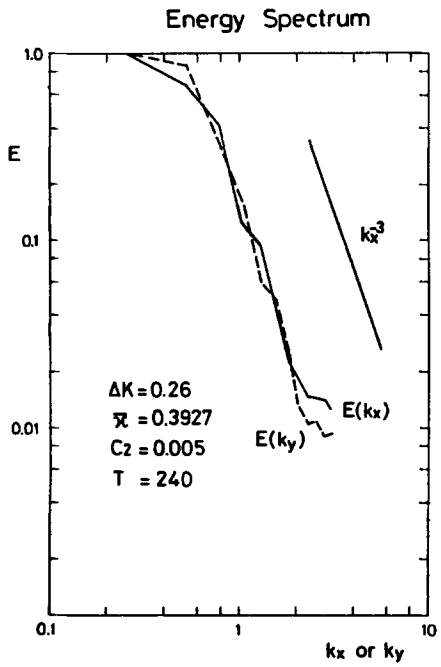

FIG. 6. Wavenumber dependency of the energy spectral. $E(k_x)$ and $E(k_y)$ are the energy spectra integrated over k_y and k_x, respectively.

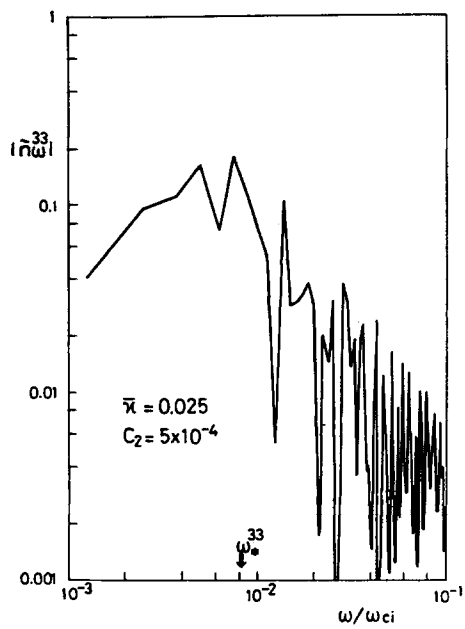

FIG. 8. The frequency spectrum of the number density fluctuation for the fixed wavenumber (3,3).

that found earlier for collisionless drift-wave turbulence.[6] A typical result of the saturated wavenumber spectrum is shown in Fig. 6. The wavenumber spectrum at large k is very close to the two-dimensional Kolmogorov–Kraichnan spectrum, $E_k \simeq k^{-3}$. This spectrum corresponds to the inertial range of enstrophy, thus the energy does not cascade in this range.

The density fluctuation and the potential fluctuation corresponding to Fig. 1 is shown in the real space (x-y space) in Fig. 7. Deviation from the Boltzman distribution, $n = \phi$, is clearly seen but the phase angle between n and ϕ is fairly small.

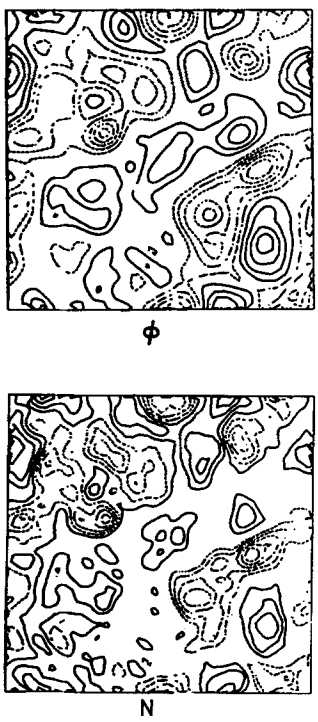

FIG. 7. The potential contour (ϕ) and number density contour (N) in x-y plane.

The frequency spectrum of the number density fluctuation for a fixed value of $\mathbf{k} = \mathbf{k}_0$, $|n_{\mathbf{k}_0\omega}|$, is shown in Fig. 8 for $\mathbf{k}_0 = (0.59, 0.59)$. It is obtained by applying the fast Fourier transform to the local density fluctuation over a time interval after the saturation. Here ω_*^{33} is the drift-wave frequency $k_y\bar{\kappa}/(1 + k^2)$ for $\mathbf{k} = \mathbf{k}_0$. The parameters of $\bar{\kappa} = 0.025$ and $C_2 = 5 \times 10^{-4}$ are close to the Caltech Research Tokamak experiment.[1,11] The frequency spectrum for a larger value of $\mathbf{k}$ was also studied and found to be broader than Fig. 8. The qualitative features of the broad spectrum peaked near $\omega \lesssim \omega_*$ agree well with the experimental observations.[1]

A spatially uniform particle flux in the x direction, $\bar{\Gamma}(t) = \langle nv_x \rangle$, appears, since $\bar{\kappa}$ is taken to be constant. $\bar{\Gamma}(t)$

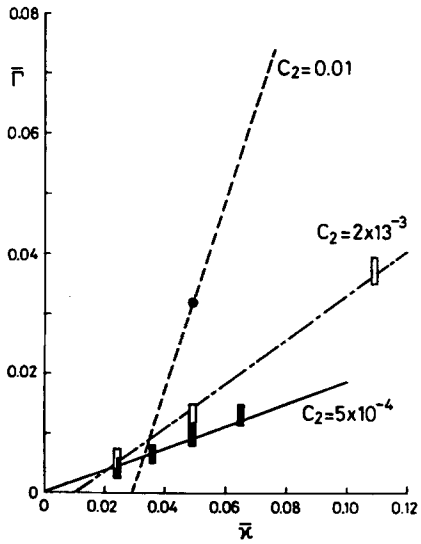

FIG. 9. Dependency of the normalized particle flux $\bar{\Gamma}$ across the magnetic field on $\bar{\kappa}$. For a sufficiently small value of C_2, $\bar{\Gamma} \propto \bar{\kappa}$ is observed to a small (realistic) value of $\bar{\kappa}$.

grows in time and approaches to a stationary level as the instability saturates. The stationary particle flux $\bar{\Gamma}$ is also found to increase linearly with $\bar{\kappa}$ as shown in Fig. 9. For a large viscosity case, the turbulent particle flux also disappears in the small $\bar{\kappa}$ regime similar to $E_{\rm sat}$ in Fig. 3. For a small viscosity case, $C_2 = 5\times 10^{-4}$,

$$\bar{\Gamma} \simeq 0.2\bar{\kappa} \tag{21}$$

is found. This flux corresponds to a diffusion coefficient D given by

$$D = \Gamma_0/\kappa n_0 = 0.2T_e/eB_0, \tag{22}$$

which is the Bohm diffusion with a coefficient 1/5. The absolute value of the particle flux is smaller than the previous estimation[11] obtained for a larger value of $\bar{\kappa}$.

Now we discuss the scaling for the saturated energy, $E_{\rm sat} \propto \bar{\kappa}$. In the energy cvonservation relation (11), the dominant contribution to the energy growth in the growing phase of the instability is attributed to the last term of the right-hand side. Therefore, approximately

$$\frac{\partial E}{\partial t} \simeq \bar{\kappa}\bar{\Gamma} \tag{23}$$

holds in this phase. The saturated energy is then estimated from

$$E_{\rm sat} \simeq \bar{\kappa}\int_0^{t_{\rm sat}} \bar{\Gamma}\, dt. \tag{24}$$

We have checked the saturation time $t_{\rm sat}$ from the numerical results and found that it is inversely proportional to $\bar{\kappa}$ as is seen from Fig. 10. Therefore, the saturation level is proportional to $\bar{\kappa}$, provided $\bar{\Gamma} \propto \bar{\kappa}$.

Next we discuss the choice of C_1 and the relevant scaling for $E_{\rm sat}$ and $\bar{\Gamma}$. When the plasma becomes collisionless, $\nu_e \lesssim v_{T_e}/qR$, C_1 becomes large, since C_1 is inversely proportional to resistivity η. To study this effect we put $C_1 = 1.0$ for all perturbations which is larger than the value given by the relation (16). This choice corresponds to a fixed parallel wavenumber k_z. For $\bar{\kappa} \lesssim 0.32$ with $C_2 = 0.025$, the resistive drift wave instability is suppressed by the last term which is proportional to C_1C_2 of the linear dispersion relation (13). The interesting result found in the numerical calculations is that when C_1 is kept to be large in the long wavelength regime, where the wave energy concentrates by the inverse cascade (see Fig. 11), the density and the potential fluctuations followed closely to the Boltzman distribution. Because of this the particle transport became very small. On the contrary, the choice of (16) gives a smaller value of C_1 in the long wavelength regime, since $C_1 \propto k^2 k_y \bar{\kappa}$, and the deviation from the Boltzman distribution appears as was seen in Fig. 7.

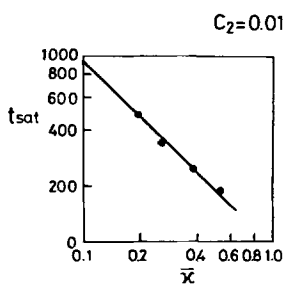

FIG. 10. The time needed for saturation $t_{\rm sat}$ as a function of $\bar{\kappa}$.

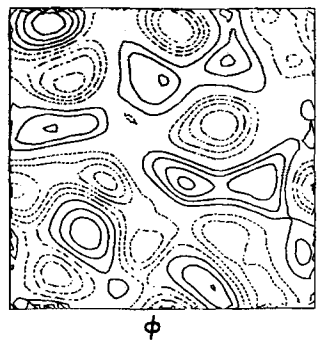

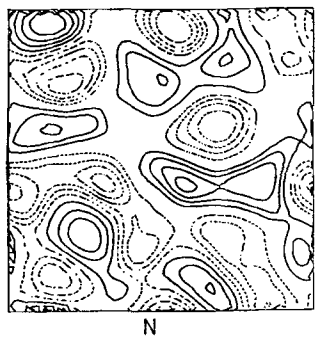

FIG. 11. The potential (ϕ) and number density (N) contour for a case with a large value of C_1.

As an alternative choice, we also tried $C_1 = 4\bar{\kappa}$. In this case we could not find a simple relation between $E_{\rm sat}$ and $\bar{\kappa}$ or $\bar{\Gamma}$ and $\bar{\kappa}$ as shown in Fig. 12. In Fig. 12, the dotted line is the same line as shown in Fig. 4. For the case of $C_1 = 4\bar{\kappa}$, $C_2 = 0.01$, and $\bar{\kappa} = 0.3927$, the saturated wave energy spectrum is shown in Fig. 13. The wave energy spectrum $E(k_y)$ shows a weak deviation from k_y^{-3} spectrum.

These results suggest that the saturation levels of E and $\bar{\Gamma}$ depend on the choice of the parameter C_1, and there exists a general tendency that the particle transport decreases for a larger value of C_1 in the long wavelength regime. Only for the choice of C_1 such that the growth rate is maximized the Bohm diffusion appears.

Finally we present the effect of the ion Landau damping term [the third term of the right-hand side of Eq. (6)]. Since the ion Landau damping appears only for a low-frequency mode such that $v_{T_i}/qR \simeq \omega_*$, we added the C_3 term only to the mode with the smallest $|k_y|$. In this case the inverse cascade process in the small k_y direction is changed, since the

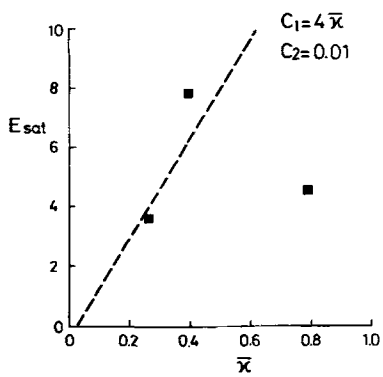

FIG. 12. Dependency of the saturation energy on $\bar{\kappa}$ for $C_1 = 4\bar{\kappa}$.

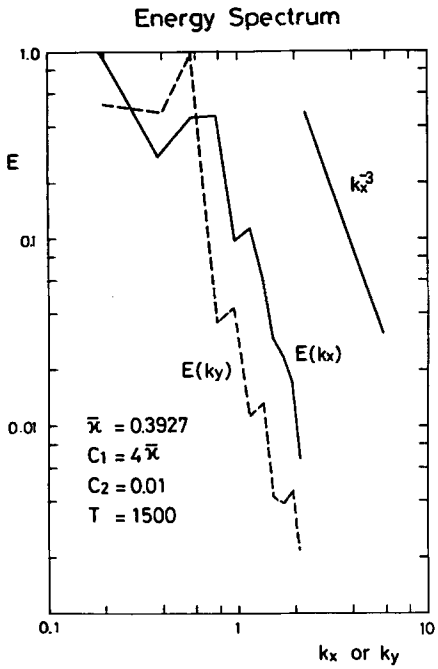

FIG. 13. The wavenumber dependency of the energy spectra for $C_1 = 4\bar{\kappa}$.

energy accumulation in the smallest $|k_y|$ modes is limited by the ion Landau damping. The white circles in Fig. 4 show the numerical results for $C_3 = 0.01\bar{\kappa}$. The saturated wave energy increases as compared with that of $C_3 = 0$. The fact that the saturation level increases is easily understood from the energy conservation law in which C_3 term is included. It is clear from Fig. 4 that the deviation between the cases with and without the Landau damping becomes increasingly small for a smaller value of $\bar{\kappa}$. This finding indicates that the effect of the ion Landau damping on the particle transport and saturated energy level is negligible for $\bar{\kappa} \lesssim 0.1$.

IV. SUMMARY AND COMPARISON WITH EXPERIMENTS

To compare our results with experimental results, let us take the example of the Caltech Research Tokamak[1] ($R = 45$ cm, $a = 15$ cm, $B_T = 4$kG, $T_{edge} \simeq 25$ eV, $n_{edge} \simeq 10^{12}$ cm^{-2}, the plasma is marginally collisional), then $c_s = 5 \times 10^6$ cm/sec, $\rho_s = 0.13$ cm. Our numerical results for the small viscosity cases given from Fig. 5 and 9

$$E_{sat} \simeq 1.3\bar{\kappa},$$

and

$$\bar{\Gamma} \simeq 0.2\bar{\kappa}.$$

Hence if we choose $\kappa \simeq 1/3$ cm^{-1} near the edge, $\bar{\kappa} \simeq 0.04$. This gives the particle flux $\Gamma = \bar{\kappa} n_0 c_S \simeq 5 \times 10^{16}$ cm^{-2} sec^{-1}, while the saturation energy $E_{sat} \simeq 0.07$. Since $\frac{1}{2} \Sigma |n_k|^2$ is found to be 75% of E_{sat}, this gives $|n_1/n_0| \simeq 0.22$. Both of these values are in fact in good agreement with the observation.[2]

The major difference of the present result from the other theory of the edge turbulence[15] exists in the fact that the present turbulence gives $|n_1/n_0| \simeq |e\phi/T_e|$, while the other theory based on the magnetohydrodynamic rippling mode gives $|e\phi/T_e| \gg |n_1/n_0|$.[15] The experimental result of the Cal Tech Tokamak favors the present result in this respect. In addition, the present result does not depend on the presence of a plasma current (while that for the rippling modes does). Thus the study of edge turbulence in stellerators or heliotrons is important to clarify the difference. In fact the preliminary results of density fluctuation measurements in an edge region of the Heliotron E at Kyoto University reveal a large level of density fluctuations of $\simeq 20\% \sim 30\%$.

The most important discovery in the present analysis is that both the particle flux and the saturation energy scale like κ, rather than κ^2 as often believed for collisionless drift wave turbulence.[14] This scaling depends crucially on the choice of the parameter C_1 ($\simeq k_z^2/\eta$). The obtained results originate when C_1 is chosen to be proportional to the linear drift wave frequency for each value of the perpendicular wavenumber such that the growth rate is maximized. Such a choice can be made possible if the plasma is collisional. Dependence of the saturation energy on the quantity $\bar{\kappa}$ leads to the relative density fluctuation n_1/n_0 being proportional to $\sqrt{\bar{\kappa}}$. This gives the density fluctuation on the order of 10% in contrast to the case when $n_1/n_0 \simeq \bar{\kappa}$, where the density fluctuation becomes on the order of 1%. If the collisionless drift wave instability gives $n_1/n_0 \simeq \bar{\kappa}$ as suggested by many authors, the present result explains why n_1/n_0 increases toward the edge. With respect to the dependence of Γ on C_2, it should be noted that the tendency of increasing Γ as C_2 is increased occurs only in a limited range of $C_2/\bar{\kappa}$. If $C_2 \gg \bar{\kappa}$, Γ decreases as C_2 is increased, while if $C_2 \ll \bar{\kappa}$, Γ increases as C_2 is decreased. Hence the relation $\bar{\Gamma} \propto \bar{\kappa}$ is valid in this limited range of C_2. In addition, as C_2 is reduced the mesh size (k_{max}^{-1}) should be reduced accordingly to obtain reliable results.

The fact that the particle flux Γ is proportional to κ is responsible to the generation of the Bohm diffusion. This result is also the consequence of the choice of k_z^2 to maximize the growth rate. Bohm diffusion is in fact observed in many experiments at tokamak edges.[2,16] Bohm diffusion near the edge, however, is not so dangerous because $D \propto T_{edge}$, where T_{edge} is generally small.

Since the Bohm diffusion is a maximum possible diffusion, one can imagine that the particle transport in the bulk region is controlled by the Bohm diffusion near the edge. Since particle flux obtained depends only on the local parameter near the edge (which maybe controlled by the wall conditions rather than the bulk parameters), $\Gamma = \text{const}$ gives the particle confinement time to be proportional to the number density of the bulk plasma, a scaling somewhat similar to the Alcator scaling.

Finally we note that if in fact $\Gamma \propto \bar{\kappa}$ in a collisional plasma and $\Gamma \propto \bar{\kappa}^2$ in a collisionless plasma, the recently discovered H-mode[12] in a tokamak plasma may be explained by an improved plasma confinement near the edge when the edge becomes collisionless due to the increased temperature in the H-mode operation.

ACKNOWLEDGMENTS

The authors appreciate useful discussions with P. K. Kaw, C. M. Surko, H. Takayasu, T. Taniuti, and S. Zweben.

The travel expenses for one of the authors (A. H.) to visit Kyoto University for this work were supported by the Yamada Foundation and the U.S. Department of Energy.

[1]S. J. Zweben, P. C. Liewer, and R. W. Gould, J. Nucl. Mater. **111**, 39 (1982).
[2]S. J. Zweben and R. J. Taylor, Nucl. Fusion **23**, 513 (1983).
[3]C. M. Surko and R. E. Slusher, Phys. Rev. Lett. **40**, 400 (1978).
[4]E. Mazzucato, Phys. Rev. Lett. **48**, 1828 (1982).
[5]D. Fyfe and D. Montogomery, Phys. Fluids **22**, 246 (1979).
[6]A. Hasegawa, Y. Kodama, and C. G. Maclennan, Phys. Fluids, **22**, 2122 (1979).
[7]A. Hasegawa and K. Mima, Phys. Fluids **12**, 87 (1978).
[8]R. H. Kraichnan, Phys. Fluids **10**, 1417 (1967).
[9]R. E. Waltz, Phys. Fluids **26**, 169 (1983); and General Atomic Report No. GA-A16943 (unpublished).
[10]P. W. Terry and W. Horton, Phys. Fluids **26**, 106 (1983).
[11]A. Hasegawa and M. Wakatani, Phys. Rev. Lett. **50**, 682 (1983).
[12]F. Wagner, G. Becker, K. Behringer, D. Campbell, A. Eberhagen, W. Engelhardt, G. Fussmann, O. Gehre, J. Gernhardt, G. v. Gierke, G. Haas, M. Huang, F. Karger, M. Keilhacker, O. Klüber, M. Kornherr, K. Lackner, G. Lisitano, G. G. Lister, H. M. Mayer, D. Meisel, E. R. Müller, H. Murmann, H. Niedermeyer, W. Poschenrieder, H. Rapp, H. Röhr, F. Schneider, G. Siller, E. Speth, A. Stäbler, K. H. Steuer, G. Venus, O. Vollmer, and Z. Yü, Phys. Rev. Lett. **49**, 1408 (1982).
[13]F. L. Hinton and C. W. Horton, Phys. Fluids **14**, 116 (1971).
[14]B. B. Kadomtsev, *Plasma Turbulence* (Academic, New York, 1965), p. 98.
[15]B. A. Carreras, P. W. Gaffney, H. R. Hicks, and J. D. Callen, Phys. Fluids **25**, 1231 (1982).
[16]Y. Gomay, N. Fujisawa, M. Maeno, N. Suzuki, K. Uehara, T. Yamamoto, and S. Konoshima, Nucl. Fusion **18**, 849 (1978).